

Does a Teleconnection between Quantum States account for Missing Mass, Galaxy Ageing, Lensing Anomalies, Supernova Redshift, MOND, and Pioneer Blueshift?

Charles Francis

Empirical implications of a teleparallel displacement of momentum between initial and final quantum states, using conformally flat *quantum coordinates* are investigated. An exact formulation is possible in an FRW cosmology in which cosmological redshift is given by $1 + z = a_0^2/a^2(t)$. This is consistent with current observation for a universe expanding at half the rate and twice as old as indicated by a linear law, and, in consequence, requiring a quarter of the critical density for closure. After rescaling Ω so that $\Omega = 1$ is critical density in the teleconnection model, it is found that for given cosmological parameters, Ω , Ω_k and Ω_Λ , luminosity distance is a factor $\sqrt{1 + z}$ greater than in the corresponding standard model. Best fits to data from the SuperNova Legacy Survey for a flat space Λ cosmology is $\Omega = 1.07$ and for a $\Lambda = 0$ cosmology, $\Omega = 1.15$. It will require many observations of supernovae at $z > 1$ to eliminate either the standard or teleconnection magnitude-redshift relation. Quantum coordinates exhibit an acceleration in time, resulting in the anomalous Pioneer blueshift and in the flattening of galaxies' rotation curves. These appear as optical effects and do not affect classical motions. Milgrom's phenomenological law (MOND) is precisely obeyed. A no CDM teleconnection model resolves inconsistencies between galactic profiles found from lensing data, rotation curves and analytic models of galaxy evolution.

Key Words: Key Words: Cosmology: cosmological parameters, theory, dark matter, distance scale; Galaxies: haloes, kinematics and dynamics.

1 Background

There is growing concern in Cosmology about unexplained empirical phenomena. The standard model of accelerating expansion is successful in matching parameters to observation, but, while there is no true reconciliation between general relativity and quantum mechanics, science should remain open to the prospect that these phenomena may have some deep underlying reason in new physics. The concept of a teleconnection arose from theoretical research into the foundations of quantum theory (Francis, 2005), but the essential tests of a new model of physics are whether the model is consistent with data, whether it gives accounts of observed phenomena which the standard model has been unable to explain, and whether it makes predictions about future tests which further distinguish it from the standard model.

It is known on theoretical grounds that new physics is required to reconcile general relativity and quantum theory (e.g Dirac, 1964). For example, Eppley and Hannah (1977) showed the necessity of a quantum treatment of gravity. Einstein (1930) suggested that the affine connection used in general relativity might be replaced with a teleparallel connection. Such a replacement can be motivated in the orthodox interpretation of quantum mechanics; if it does not make sense to talk of position between measurements then it is also without sense to talk of geodesic motion of a photon emitted from a distant star and detected on Earth. Individual detection of photons from distant stars suggests that quantum theoretical effects may come into play. If this is the case we cannot be certain of the analysis of redshift without first having a rigorous formulation of

quantum motions in curved space time. Here we consider the wave function in a quantum formulation, as a probabilistic relationship between an initial and a final state, respectively the emission and detection of a photon. The connection is defined between the coordinate systems used to describe these states and will be called a *teleconnection*.

A new model of physics should adhere to fundamental principles such as the cosmological principle, the special and general principles of relativity, the uncertainty principle and the principle of superposition. This paper carries out a preliminary investigation of the empirical implications of a modification to general relativity adhering to these fundamental principles. Standard general relativity and quantum mechanics are assumed, except that the affine connection is replaced and wave functions are defined using *quantum coordinates*, not in curved spacetime. The tests described here could have falsified the model, but if anything the reverse is the case as there is no consistent standard model for CDM haloes or explanation for Pioneer blueshift. An initial analysis of current astronomical data is consistent with a universe with close to critical density and no cold dark matter or cosmological constant, but with no apparent timescale problem (table 1). As a bonus the teleconnection models the flattening of galaxies' rotation curves and Pioneer blueshift, without requiring either a change to Newtonian dynamics or galactic haloes and a revised relationship between redshift and age offers the prospect of a reconciliation between observation and galaxy evolution models. In the instance of galactic rotation curves testing has been done, not through direct statistical analysis, but by deriving a general law (MOND) already established from statistical analysis. The magnitude-redshift relation has been analysed by Bob Day using data sets from Riess (2004) and Astier (2005). The new relation is sufficiently close to that of the standard model that it will require many observations of supernovae at redshifts $z > 1$ to distinguish empirically between the curves.

A heuristic description of the teleconnection is given in section 2. For this purpose a closed universe will be discussed. Other models are possible, but this simple model is consistent with observation and should be sufficient to understand the empirical tests described in sections 3 to 8. A formal treatment is deferred to appendix A, showing that the teleconnection can be consistently defined in an FRW cosmology, that the prescription reduces to the standard affine connection in the classical correspondence, and that geodesic motion obtains for classical particles and for a beam of light.

Table 1: Properties Compared

Connection	Affine	Teleconnection
Expansion rate	$\dot{a}/a = H$	$\dot{a}/a = H/2$
Critical density ($\Omega = 1$)	$3H^2/8\pi G$	$3H^2/32\pi G$
Topology	Open	Any
Ω ($\Omega_k = 0$)	0.263 ± 0.05	1.07 ± 0.05
Ω ($\Omega_\Lambda = 0$)	—	1.15 ± 0.21
Ω_B	$0.025 \sim 0.05$	$0.1 \sim 0.2$
Current age	~ 14 Gyr	17 to 20 Gyr
Age at $z = 6$	~ 0.7 Gyr	~ 4.5 Gyr
Baryon:Non-baryon	$\sim 15:1$	$4:9:1$
CDM haloes	inconsistent	absent
Pioneer blueshift	unexplained	$a_P = H_0 c$
MOND	CDM	$a_M = H_0 c/8$
Wave motion	curved space?	flat space
Classical motion	geodesic	geodesic
Luminosity distance	d_L	$\sqrt{1+z}d_L$
Distance modulus	μ	$\mu + 2.5\log(1+z)$
First order comparison:		
Affine:	$\mu \approx 5\log z + 1.086(1-q)z$	
Teleconnection:	$\mu \approx 5\log z + 1.086(2-q)z$	

2 The Teleconnection

This is not a teleparallel theory using the Weitzenböck connection (see e.g. Arcos and Pereira, 2004). The teleconnection applies between initial and final states in the quantum theory. It does not apply when there is an intermediate measured state. In the classical correspondence, when continuous measurement is possible in principle, torsion will be removed and gravity will be described by curvature, as is normal in general relativity.

In general relativity it is assumed that photon momentum is parallel transported through large distances. This assumption takes no account of the propagation of a photon wave function in a curved space-time, which would imply that a photon of precise momentum at time of emission would not have precise momentum at absorption. Here it is assumed that there exists a coordinate space in which plane wave states are defined, that is one with metric given by (3.2). Momentum at source is teleparallel to momentum at detection, and this determines a connection between coordinate systems used to describe the initial and final states.

As in general relativity there is no local meaning to expansion because length is defined locally, by an empirical procedure using local matter. To talk about expansion we have to compare a length scale defined here and now, using here and now clocks and rulers, with a length scale defined at some time in the past. In practice we can do this by studying light from the past and analysing redshift *provided* that we know how light behaves. The definition of a teleconnection assumes that if momentum has a precise value at one place and time then it also has a precise value other places and times and is empirically justified in so far as observation yields precise values for cosmological redshift after allowing for dispersion due to dust or other known factors. This is a fundamental assumption in this model, of equal importance to the assumption of the constancy of the speed of light in special relativity. Like that assumption, if it were dropped we would be left, not with a different theory, but with no known consistent theory.

Let Alf be an observer on a space craft or a distant planet, and let Beth be an observer on Earth, such that Alf can signal to Beth. At the time of emission of a photon passing from Alf to Beth, Alf defines synchronous co-ordinates in 3 dimensions at constant cosmic time t , using proper distance as the radial coordinate (figure 1). In a closed cosmos the universe can mapped onto a finite space, which will be called *Alf's map*. Beth defines *Beth's map* in exactly the same way, to the same scale, at the time of detection of the photon, cosmic time t_0 . For a closed universe in three dimensions Alf's and Beth's maps are spherical. Let $a(t)$ be the scale factor and let $a_0 = a(t_0)$. If the universe expands during the time of travel of the photon from Alf to Beth, then Beth's map is larger than Alf's map by a factor $a_0/a(t)$.

To formulate a quantum theory of the motion of a photon from Alf to Beth from an initial state $|f(t)\rangle$ at Alf's cosmic time to a final state $|f(t_0)\rangle$ at Beth's cosmic time, Beth enlarges Alf's map by the factor $a_0/a(t)$. She defines the teleconnection such that photon momentum is represented by a vector of equal magnitude and direction on Beth's map and on Alf's enlarged map (figure 2). Alf and Beth now define four dimensional maps by considering all the times and positions where the other might be, with the time axis scaled so that light is shown at a constant angle necessary to plane wave motions (figure 3). These are Penrose diagrams in each time-radial plane. In these coordinates we define *coordinate space vectors*, designated with a bar as in (A1.2). In these coordinates plane wave states are defined by

$$|\bar{p}\rangle = \left(\frac{1}{2\pi}\right)^{3/2} \int_{-\pi}^{\pi} d^3x e^{i\bar{x} \cdot \bar{p}} |\bar{x}\rangle \quad (2.1)$$

and the wave function is strictly invertible

$$\langle \bar{x} | f \rangle = \left(\frac{1}{2\pi}\right)^{3/2} \int_{-\pi}^{\pi} d^3\bar{p} \langle \bar{p} | f \rangle e^{-i\bar{x} \cdot \bar{p}} \quad (2.2)$$

Thus, for a closed FRW cosmology, there is a precise formulation of quantum mechanics in which plane waves are states and not distributions. It will be observed that Alf's and Beth's formulations of quantum theory are different. This is legitimate in the orthodox interpretation in which wave functions do not represent a physical wave property, and are merely used to calculate probabilities.

Beth can compare the scale of her map to that of Alf's map by studying red shift. There are two scaling effects. First Alf's map has been enlarged by a factor $a_0/a(t)$. In addition, the scaling on the map changes as you move from one point to another, giving another factor $a_0/a(t)$ from (A1.2). Thus, the model predicts a net factor for cosmological redshift which varies with the square of the expansion parameter:

$$1 + z = a_0^2/a^2. \quad (2.3)$$

(2.3) applies to a quantum motion between an initial state, $|f(t)\rangle$, at time t , and a final state, $|f(t_0)\rangle$, at time t_0 , when it is not meaningful to describe the intervening state in terms of measured physical quantities. In the classical correspondence time is taken as a continuous variable and motion may be described as a sequence of measured states $|f(t_i)\rangle$ at instances $t_i \in T$ for $i = 1, \dots, n$ such that $\forall i \ 0 < t_i - t_{i+1} < \chi$ in the limit in which χ tends to zero. The state at any instant may be regarded as an initial state, and the state at the next instant may be regarded as a final state for that part of the motion. The final state then becomes the initial state for the next part of the motion. At each instant t_i the coordinate system must be rescaled such that the quantum

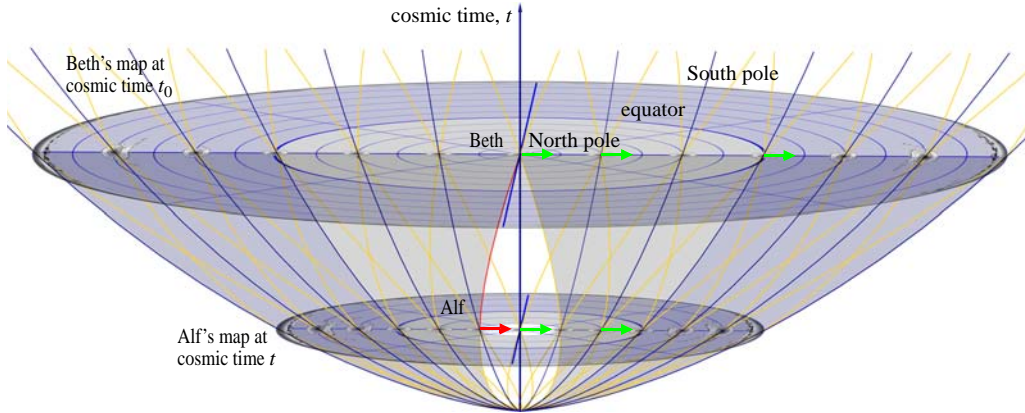


Figure 1: Alf and Beth's maps at constant cosmic time with radial coordinate equal to proper distance. Alf and Beth are here drawn in different galaxies. For convenience Beth's galaxy is taken as the origin of both maps. One dimension is suppressed, so the maps are spherical in three dimensional space. Identical galaxies are shown on geodesics emanating from the big bang in the $x-t$ plane. As drawn each galaxy has the same radial dimension but the galaxies acquire an increasing angular stretch towards the edge of the map. These scaling distortions are physically meaningless and can be removed by embedding the $x-y$ plane onto the surface of a sphere with Beth at the North pole. Thus local geometrical properties are everywhere the same in accordance with the cosmological principle. The circles on the maps correspond to lines of latitude at 15° and 30° intervals for Beth's and Alf's respective maps. The region corresponding to the Southern hemisphere, shaded blue, appears outside the Northern hemisphere. The outermost circumference is infinitely stretched and represents a point, the South pole. The galaxy at the South pole is so stretched that it surrounds the map. In the diagram the universe doubles in size between Alf's and Beth's cosmic time, at which point it is at half maximum expansion. The path of light is shown in yellow, with the signal from Alf to Beth shown in red. The region outside Beth's past light cone is shaded grey. A space-like radial vector has the same apparent and proper length at any point (green). In his own coordinates Alf scales a red coordinate space vector to be equal to the green physical vector.

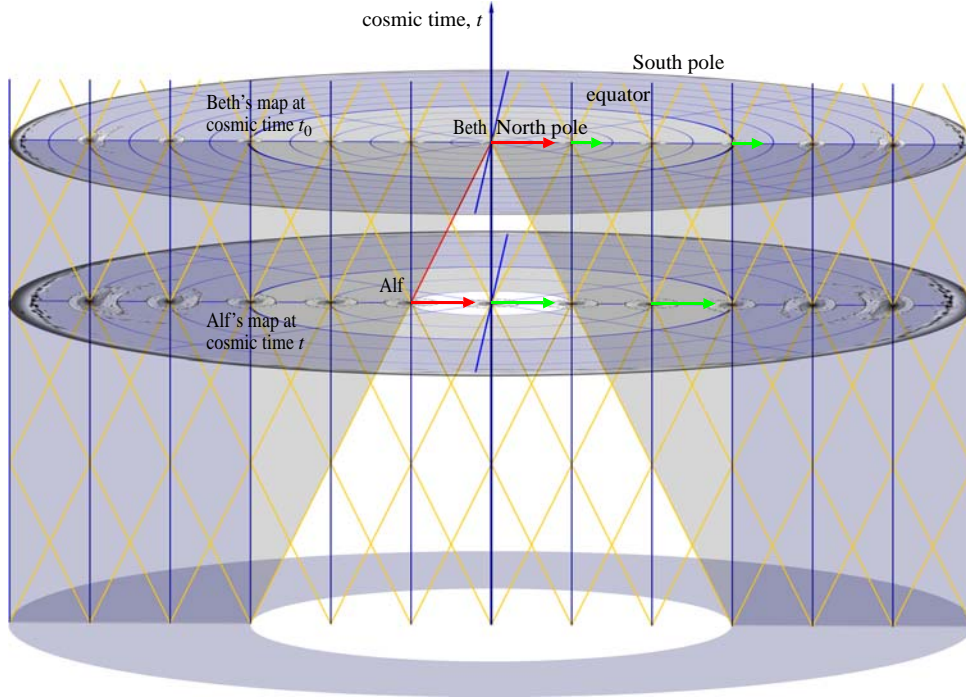


Figure 2: Beth's map of space time. The scale of Alf's map is doubled so that it is the same size as Beth's. Both the red coordinate space vector and the green physical vector on Alf's map appear twice as long in these coordinates. The time axis is also rescaled, being stretched downwards by greater amounts approaching the big bang, so that light is shown at a constant angle. This condition is necessary and sufficient for radial plane wave motions, defined using coordinate space vectors which have the same apparent length everywhere. Since the apparent length of a coordinate space vector (red) remains the same under teleparallel displacement from Alf to Beth, it's real length doubles.

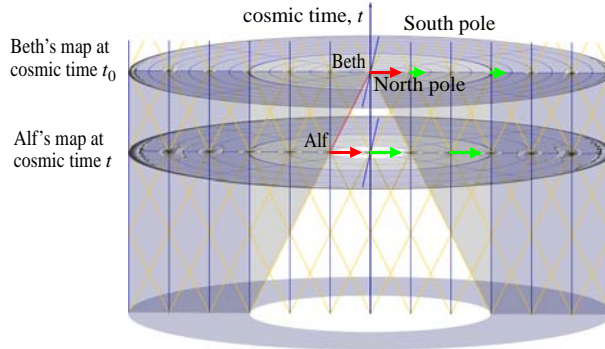


Figure 3: Alf's map of space-time is found by halving the scale of Beth's map. Beth formulates quantum theory on figure 1, while Alf formulates it on figure 2. So Beth sees a net factor of four in the wavelength of an e.m. signal sent from Alf to Beth, and the redshift is $z = 3$, not $z = 1$ as would be the case in the standard model.

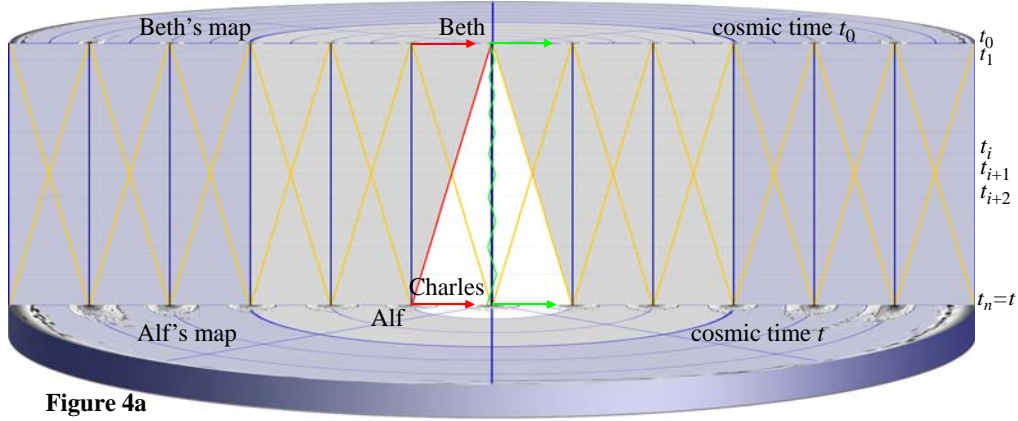


Figure 4a

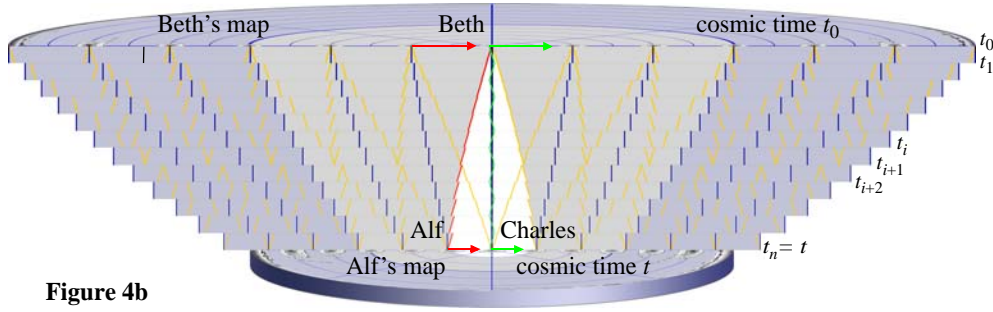


Figure 4b

Figure 4: In the classical correspondence it is possible to define the state on synchronous spacial surfaces at constant cosmic times t_i separated by a small interval. The state at any instant, t_i , may be regarded as an initial quantum state. The state at the next instant t_{i+1} may be regarded as a final state, which, after rescaling, becomes the initial state for the next part of the motion. Time evolution is described as a series of quantum steps, $\langle f(t_{i+1}) | f(t_i) \rangle$. With each rescaling of coordinates between steps, momentum is renormalised such that, at each instant t_i , conservation of momentum is preserved and the non-linearity of time seen in figure 4a is removed. In the limit, $\forall i = 1, \dots, n, t_{i+1} - t_i \rightarrow 0$, figure 1 is restored. Thus, if Beth's ancestor, Charles, had set up a trapped signal (green) in a laboratory on Beth's planet, such that its wavelength could be measured at any time, then the classical linear redshift law found from the affine connection will be measured.

theory is defined on the torus $(-\pi, \pi)^3$ (figure 4). The paths of light and of the galaxies become continuous in the limit $\chi \rightarrow 0$, in which figure 1 is recovered.

We require that momentum is conserved at each instant, i.e. that the momentum space wave function is unchanged when a final state is reinterpreted as an initial state. Momentum must be renormalised upon rescaling, which requires a factor $a(t_{i+1})/a(t_i)$. It follows that momentum is parallel displaced from t_{i+1} to t_i and that (2.3) is replaced with the usual linear law

$$1 + z = a_0/a. \quad (2.4)$$

Thus, in the classical correspondence, the teleconnection reduces to a Riemann affine connection.

3 Cosmological Redshift

When light is received from a distant object cosmological redshift is given by (2.3). For small r

$$1 + z \approx 1 + 2r\dot{a}/a. \quad (3.1)$$

Thus coordinates in which radial distance from Earth is calculated from redshift exhibit a stretch of factor half in the radial direction. Using (A1.2), the radial component of the coordinate space position vector of an object at radius r is $\bar{r} = 2r$. The time taken for a pulse of light at this distance to traverse a small angular distance $d\theta$ is $\bar{r}d\theta = rd\theta$. So there is a stretch of factor two in the angular directions (this gives 4π in a circle, which may cast light on fermion phase under rotation). Thus the metric, (A3.2), for quantum coordinates is:

$$ds^2 = a^2(4(dt^2 - d\rho^2) - \frac{1}{4}f^2(\rho)(d\theta^2 + \sin^2\theta d\phi^2)). \quad (3.2)$$

Definition: Hubble's constant, $H \equiv 2\dot{a}/a$, is read from (3.1).

It follows immediately that the rate of expansion of the universe is half that predicted by the standard model, the universe is twice as old as would be indicated by a linear law, critical density for closure is a quarter of the standard value, and that there is no apparent timescale problem for a closed FRW universe with greater than critical density and zero cosmological constant.

If observations at high red shift had revealed the expected activity of the early universe it would have falsified the square red shift law; in fact it receives support from the observation of mature galaxies at $z = 1.4$ and greater (e.g. Mullis et al., 2005; Doherty et al 2005, and references cited therein). As described by Glazebrook (2004), there is poor agreement between current theoretical models of galaxy evolution and empirical data. To explain this it has been suggested (Cimatti et. al, 2004) that the theoretical models may be inaccurate. This model presents an alternative, that a square redshift law means we have to revise the ages of red galaxies.

A value of Hubble's constant $h = 0.72$ places an upper bound on the age of the universe of eighteen billion years; at redshift 6 the universe would have been about 4.5 billion years old. The accelerations of galaxies in clusters are in the MONDian regime, and after revising the age-redshift relation, there is neither immediate evidence that CDM is necessary to explain galaxy evolution, nor strong reason to suppose that galactic evolution models are inaccurate at the resolutions and step sizes available with today's supercomputers. A detailed study is required to assess consistency between observation and theory, but this certainly appears to alleviate the difficulties. Hopefully future observation and analysis will be conclusive.

4 Lensing

The teleconnection model predicts geodesic motion for a classical ray of light so that there is no change in the prediction of bending of light around a body such as the Sun, which has known mass and for which distance can be determined by direct measurement. The analysis is quite different for a lens whose distance is determined from redshift. In this case the bending of light by the lens must be described using quantum coordinates, as given by (3.2) and seen in figure 5. Lensing is affected in two principal ways in the teleconnection model: first, in the absence of a CDM halo, lower galactic masses reduce lensing; second the use of quantum coordinates quadruples the angle of deflection as compared to standard general relativity.

Zhao et al. (2006) tested lensing in Beckenstein's relativistic MOND (TeVeS), and conclude that lensing may be a good test for CDM theories. The problem for standard no CDM theories is that, because of the lower galactic masses it is difficult to account for the amount of lensing in all cases. Zhao et al. found that "TeVeS succeeds in providing an alternative to general relativity in some lensing contexts; however, it faces significant challenges when confronted with particular galaxy lens systems". However, the empirical determination of the mass of the lensing galaxy is

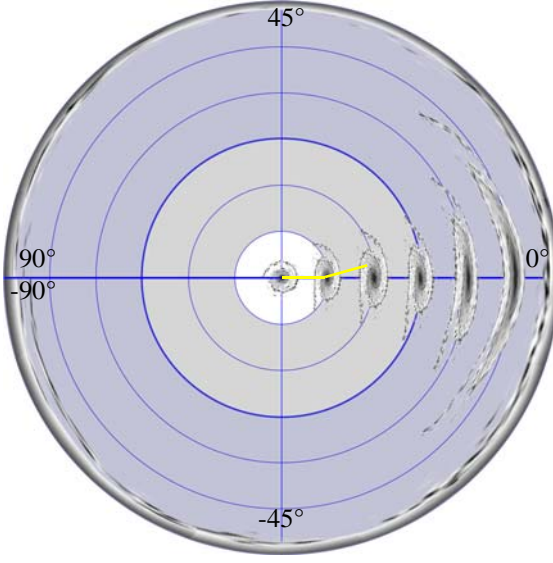


Figure 5: Alf's map in quantum coordinates. Quantum coordinates apply to wave functions and are not directly measured, except in the direction of the positive x -axis, i.e. the direction in which one is actually looking at an incoming photon. Radial distance is halved, but angular distances are doubled. This increases the deflection angle by a factor of four as compared to other no-CDM models. The diagram is discontinuous on the negative x -axis and has two parts.

not sufficiently precise to eliminate it for all choices of parameters. Each observed lens requires careful analysis, but given that the teleconnection model predicts a substantially greater angle of deflection than TeVeS it appears unlikely that the determination of lens masses will provide a definitive test at the current level of accuracy of observation.

A clearer test may be the analysis of the profile of the halo. There is now a substantial literature on lensing profiles indicating that the standard model is not consistent. According to evolutionary models dark matter halos should have steep central density cusps (e.g., Navarro, Frenk, & White 1997) but they appear not to (e.g., de Blok, Bosma, & McGaugh 2003; Swaters et al. 2003). Martel and Shapiro (2003) have examined the profile of lenses for a number of evolutionary models. While they find quantitative fits for many properties, they again find that the models do not correctly reproduce the central region. Park and Ferguson (2003) studied the lensing produced by Burkert haloes and found, "For the scaling relation that provides the best fits to spiral-galaxy rotation curve data, Burkert halos will not produce strong lensing, even if this scaling relation extends up to masses of galaxy clusters. Tests of a simple model of an exponential stellar disk superimposed on a Burkert-profile halo demonstrate that strong lensing is unlikely without an additional concentration of mass in the galaxy center (e.g. a bulge)".

Power et al (2003) also comment on discrepancies between analytic models and halo distribution required by galaxy rotation curves. In particular they state "there is no well defined value for the central density of the dark matter, which can in principle climb to arbitrarily large values near the centre". Of this result they say "there have been a number of reports in the literature arguing that the shape of the rotation curves of many disk galaxies rules out steeply divergent dark matter density profiles" and conclude that it "may signal a genuine crisis for the CDM paradigm on small scales". On the other side of the debate, Milgrom and Sanders (2005) found halo properties in Ursa Major Galaxies consistent with MOND predictions, and in a one study for which a particularly good analysis is possible, Wayth et al. (2005) found that, for the optical Einstein ring gravitational lens ER 0047-2808, lensing is consistent with a halo of the same mass distribution as the galaxy itself. This result is not consistent with either the halo distribution required to produce galactic rotation curves, or with evolutionary halo models. It is, of course, trivially consistent with both in a no CDM model.

5 Cosmological Parameters

The interpretation of redshift alters cosmological parameters but otherwise leave the classical equations of general relativity unchanged. Friedmann's equation is

$$\dot{a}^2 = \frac{8}{3}\pi G\rho_0 a_0^3/a + \frac{1}{3}\Lambda a^2 - k. \quad (5.1)$$

Normalising so that $\Omega = 1$ is critical density Ω takes on four times its standard value:

$$\Omega = 32\pi G\rho_0/3H_0^2, \Omega_k = -4k/H_0^2 a_0^2, \text{ and } \Omega_\Lambda = 4\Lambda/3H_0^2, \quad (5.2)$$

where $k = -1, 0, 1$. Then Friedmann's equation, (5.1), is,

$$\dot{a}/a = \frac{1}{2}H_0(\Omega(1+z)^{3/2} + \Omega_k(1+z) + \Omega_\Lambda)^{1/2}, \quad (5.3)$$

requiring that $\Omega + \Omega_k + \Omega_\Lambda = 1$.

Definition: Let the deceleration parameter be:

$$q \equiv -a\ddot{a}/\dot{a}^2 = -4\ddot{a}/aH^2. \quad (5.4)$$

Differentiate Friedmann's equation:

$$\ddot{a}/a = -\frac{4}{3}\pi G\rho_0 a_0^3/a^3 + \frac{1}{3}\Lambda = -\frac{4}{3}\pi G\rho_0(1+z)^{3/2} + \frac{1}{3}\Lambda. \quad (5.5)$$

Let $H_0 = H(t_0)$, $a_0 = a(t_0)$ and $q_0 = q(t_0)$. From (5.2) and (5.5),

$$q_0 = \frac{\Omega}{2} - \Omega_\Lambda. \quad (5.6)$$

A small angular displacement determined from the wave function can be regarded as a coordinate space vector. A factor of two in angular distances is removed on going from quantum to conventional coordinates, so that angular size distance is multiplied by a net factor $a_0/a(t) = \sqrt{1+z}$. This adds $2.5\log_{10}(1+z)$ to magnitude. To first order in z the magnitude-redshift relation becomes:

$$m - M \approx 5\log_{10}z + 1.086(2 - q_0)z + O(z^2) \quad (5.7)$$

(c.f. Misner Thorne Wheeler 1973, eq. 39.35b, quoted in table 1). Then if q_s is the deceleration parameter for the standard model $q_0 \approx q_s + 1$. If $\Lambda = 0$, $\Omega \approx 3\Omega_s$. In this case the error in Ω will be about three times that of the standard model. For a flat space model, $\Omega \approx \Omega_s + \frac{2}{3}$ and the error will be roughly equal to that of the standard model. For critical density, $\Omega = 1$, $\Omega_\Lambda = 0$, (5.7) is identical to first order, to the magnitude-redshift relation with $\Omega_s = 0.33$, $\Omega_{\Lambda s} = 0.67$. In practice the first order approximation, (5.7), is not adequate to accurately identify cosmological parameters. In figures 6, 7, 8 the plot for the $\Omega = 1$, $\Omega_\Lambda = 0$ model has been superimposed in green on residual Hubble diagrams by adding $2.5\log_{10}(1+z)$ to the standard plot. For $z > 0.4$ the fit is closer to $\Omega_s = 0.27$, $\Omega_{\Lambda s} = 0.73$ than it is to the $\Omega_s = 0.35$, $\Omega_{\Lambda s} = 0.65$, so for this preliminary analysis the error in the $\Lambda = 0$ model has been estimated by multiplying the estimated error in the standard fit by four.

Using Matlab, Bob Day ran χ^2 tests on the modified magnitude-redshift relation for the Riess (2004) and Astier (2005) data sets. For the Astier data he removed two outliers also removed by Astier, leaving 115 data points (figure 9). Astier minimised with respect to four variables, Ω , M , α and β . For a preliminary analysis Day used the optimum values of α and β found by Astier for the standard fit, and minimised with respect only to Ω and M . This means that χ^2 may be above the minimum for the teleconnection fit, but as the curves are very close throughout the data range it is unlikely that varying α and β will greatly affect the result. The best fit flat space standard model was $\Omega_s = 0.263$ with $\chi^2 = 113.6$. For the teleconnection flat space Λ model the best fit was $\Omega = 1.07$ with $\chi^2 = 115.1$, and for the $\Lambda = 0$ model it was $\Omega = 1.15$, $\chi^2 = 114.7$.

Using the Riess gold set data (figure 10) Day removed three outliers, including one with a high error margin. Removal of outliers reduces χ^2 but makes little difference to the prediction for

Omega. A further test was run in Quattrix modeler with six outliers removed. For 151 dof the best fit with the standard model was $\Omega_s = 0.29$ with $\chi^2 = 148.0$. The best fit with the teleconnection flat space Λ model was $\Omega = 1.17$ with $\chi^2 = 156.9$, and the best fit no Λ model was $\Omega = 1.34$ with $\chi^2 = 153.7$. The higher value of χ^2 for the teleconnection model is largely due to points at $z > 0.9$. The lensing correction to SN1977ff was removed from the teleconnection fit because it is not clear that lensing is a factor; the lensing of SN1977ff is peculiar, because two lenses are required at very precise locations to give an undistorted image of the host galaxy (Benítez et al., 2002). Given the finding of Mörtzell, Gunnarsson, & Goobar (2001) that the lensing of SN1977ff is very sensitive to ray-tracing, it seemed unwise to assume it.

The higher values of Ω for both the standard and teleconnection model may be an indication of a systematic error which may be due to selection effects or to practical measurement difficulties at $z > 0.8$, as discussed by Astier. It may be observed that the high z observations in the Riess gold set drop below both standard and teleconnection curves. With the top fifteen data points removed leaving 136 dof the best fit standard model has $\Omega = 0.235$ with $\chi^2 = 128.8$, while the teleconnection Λ model has $\Omega = 1.001$ with $\chi^2 = 130.52$ and the best fit no Λ model has $\Omega = 1.038$ with $\chi^2 = 130.46$. High z observations have the most “leverage” on the value of Ω , but there is not enough data at $z > 1$ for a statistically significant sample, and there are substantial measurement difficulties at high z . Current searches like SNLS and ESSENCE are directed at finding SN with $z < 1$. In order to eliminate either the teleconnection or the standard model it will be necessary to collect systematically a substantial body of observations at $z > 1$ and to rigorously analyse them to eliminate possible systematics.

Figure 6: Hubble diagram of SNLS and nearby SNe Ia from Astier (2005). The plot shows the residuals for the best fit to a flat, $\Omega_s = 0.26$, $\Omega_{\Lambda s} = 0.74$ cosmology. The grey curve is the standard $\Omega = 1$, $\Omega_{\Lambda} = 0$ model and the superimposed green curve is the teleconnection $\Omega = 1$, $\Omega_{\Lambda} = 0$ cosmology.

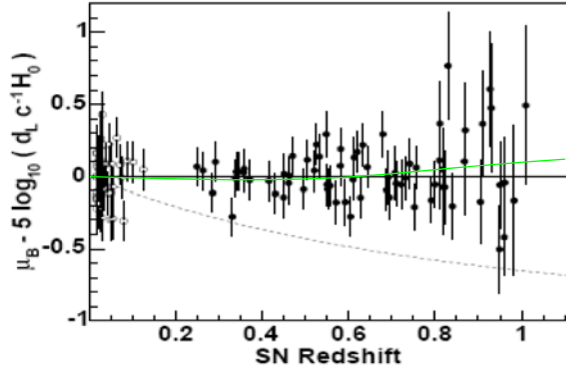
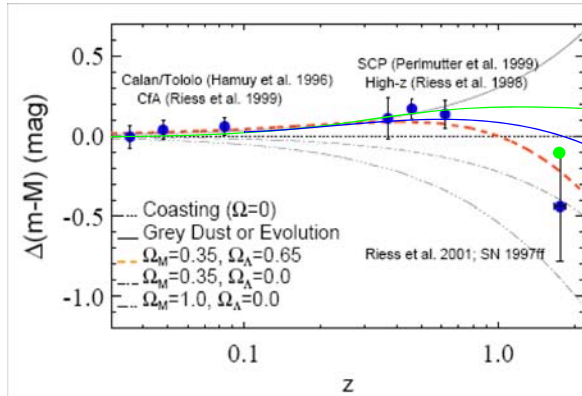


Figure 7: Hubble diagram from Filippenko (2003). SNe Ia relative to an empty, ($\Omega = 0$), universe compared with cosmological and astrophysical models (Riess et al. 2001). Low-redshift SNe Ia are from Hamuy et al. (1996a) and Riess et al. (1999a). The superimposed green curve is the teleconnection $\Omega = 1$, $\Omega_{\Lambda} = 0$ cosmology. The best fit for the flat space Λ teleconnection model with $\Omega = 1.15$ is shown in approximation in blue. The magnitude of SN 1977ff at $z = 1.7$ was adjusted for gravitational lensing (Benítez et al. 2002). The unadjusted position is shown in green.



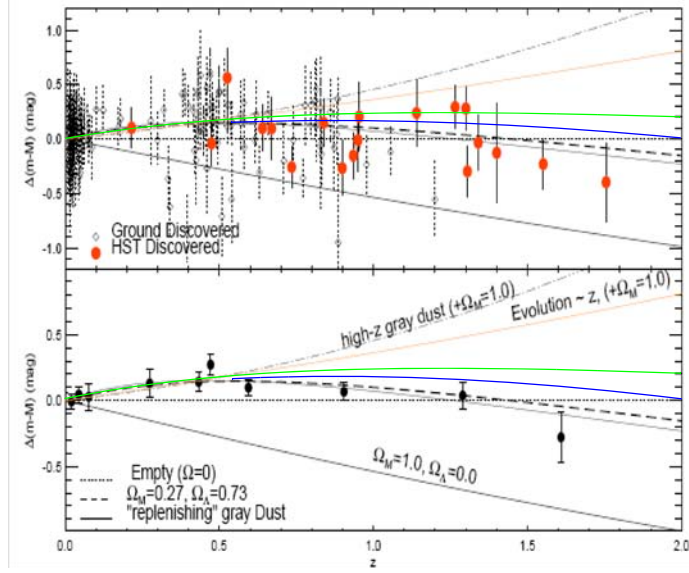


Figure 8: SN Ia residual Hubble diagram comparing cosmological models from Riess et al. (2004). Upper panel: SNe Ia from ground-based discoveries are shown as diamonds; HST-discovered SNe Ia are shown as filled symbols; SN1997ff unadjusted for gravitational lensing is shown in green. Lower panel: Weighted averages in fixed redshift bins, which are given only for illustrative purposes. Data and models are shown relative to an empty universe. The superimposed green curves are the teleconnection $\Omega = 1$, $\Omega_\Lambda = 0$ cosmology. The best fit for the flat space Λ teleconnection model has $\Omega = 1.15$ and lies just below the green curve, as shown in approximation in blue. For $z > 0.9$ the bulk of the data lies below both the standard and teleconnection curves, which may be indicative of a systematic.

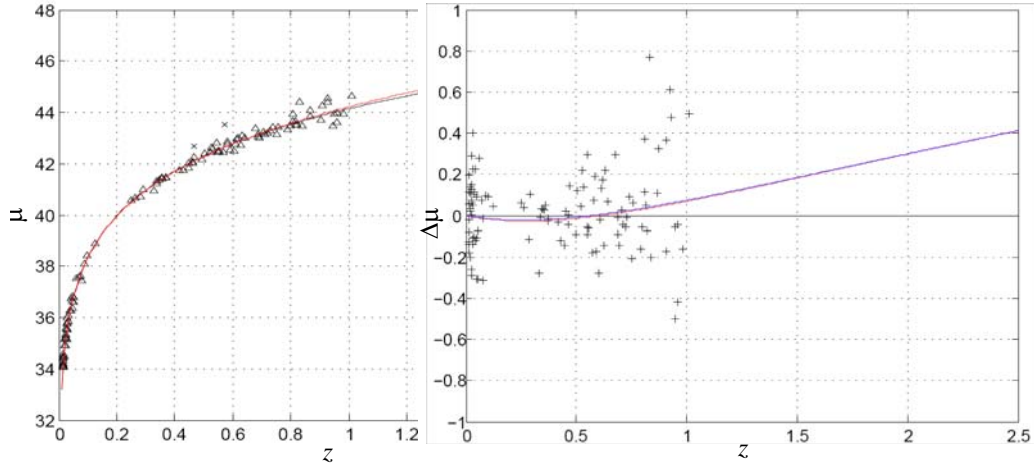


Figure 9: Hubble diagram using data from Astier (2005), 115 data points, two outliers removed as noted by Astier. The best fit for the standard model (black) has $\Omega_s = 0.263$ with $\chi^2 = 113.6$. The plot for the teleconnection flat space model $\Omega = 1.07$, has $\chi^2 = 115.1$ (red) and is almost indistinguishable from that for the $\Lambda = 0$ model with $\Omega = 1.15$ and $\chi^2 = 114.7$. The right hand panel shows residuals to the best standard fit, $\Delta\mu = 0$. The teleconnection model with $\Lambda = 0$ is shown in blue.

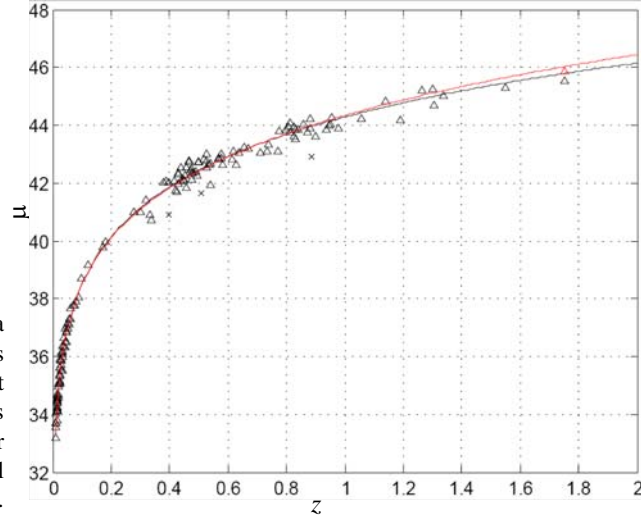


Figure 10: Hubble diagram using data from Riess (2004) with three outliers removed; 154 data points. The best fit for the standard model (black) has $\Omega_s = 0.29$ with $\chi^2 = 159.6$, and for the teleconnection flat space Λ model (red) has $\Omega = 1.15$ with $\chi^2 = 171.2$.

6 Anomalous Pioneer Blueshift

Consider a wave packet for a particle of zero momentum and at a distance r from an observer moving with the cosmic fluid at time t_0 , on a spacecraft in empty space where gravity can be ignored. The coordinate space displacement vector of the particle from the observer is a horizontal arrow of constant length. By (2.3), the scaling distortions in quantum coordinates are such that the actual displacement represented by the coordinate space displacement vector is greater at time t_0 than it was at time $t < t_0$, by a factor a_0^2/a^2 . But the particle is also on a geodesic moving with the cosmic fluid. So its actual displacement is greater by a factor, a_0/a . Then the motion of the wave packet and that of the particle diverge, and the wave packet accelerates toward the observer. The effect is clearly seen in figure 4b. The red arrow is stretched, i.e. momentum is red shifted with each quantum step, tending to parallel transport in the limit of small step size. In figure 4b the geodesics from figure 1, i.e. the rays of light and the galaxy path are broken into small segments. Cosmological redshift derives from the way the breaks take the segments outwards. Each segment is directed inwards compared to geodesic motion. This is a wave function effect seen in the anomalous Pioneer blueshift.

For some years the Pioneer spacecraft have been sending back Doppler information interpreted as an anomalous acceleration toward the sun (Anderson et al., 2002). No accepted explanation has been given for the anomalous blueshift, but if it were not observed it would be fatal to this model. Although what is measured is anomalous blueshift, JPL elected to express their result in the form of an equivalent classical acceleration, $a_p = 8.74 \pm 1.33 \times 10^{-8} \text{ cms}^{-2}$. Anderson remarks that the blueshift is equivalent to an “acceleration in time” equal to the Hubble constant, but rejects acceleration in time because, using conventional physics, it is incompatible with ranging data. This is not true of the teleconnection model. A laboratory moving with respect to the cosmic fluid uses locally Minkowski coordinates, which can be transformed locally to comoving coordinates and extended globally to coordinates with metric given by (3.2). Then the time coordinate obeys (A3.4), and exhibits acceleration with respect to proper time. Acceleration in time is seen in figure 4a, in which discs of constant proper time become less deep as quantum time increases. The value of the acceleration in time is $H_0/2$ but blueshift is doubled in (3.1), so that the resultant shift is the same. The equivalent acceleration, $a_p = H_0 c$, is consistent with recent determinations of Hubble’s constant

Acceleration in time leads to a prediction of blueshift simulating constant acceleration toward the origin of coordinates, that is toward the observer on Earth. This is a quantum effect; consistent with NASA's findings, there is no corresponding classical acceleration and planetary motions are unaffected. A future test is planned which will determine whether the acceleration is toward the Sun, toward the Earth, in the direction of motion of the craft, or along the spin axis (Nieto et. al. 2004). This information may also be discovered from reanalysis of the archive of Pioneer transmissions (Turyshev et al, 2006). If the direction is not toward the Earth the test will falsify this model.

There is a fundamental difference between the predictions of the model for bound and hyperbolic trajectories. In an elliptical orbit the path is cyclic and can be determined in principle by direct measurement. Then inward acceleration is measured not as a drift but as an apparent change in orbital velocity. This is in accordance with the finding of Turyshev et al. (2006), "The Pioneer 11 data also indicated that the anomaly ... appears to be amplified (or turned on) at a distance of ~ 10 AU from the Sun. This is approximately when the craft flew by Saturn and entered an hyperbolic, escape trajectory".

7 Flattening of Galaxies' Rotation Curves

The Pioneer blueshift is present in the observation of distant galaxies, and precisely accounts for flattening of galaxies' rotation curves consistent with MOND, the phenomenological law found by Milgrom (1994) which replaces the inverse square law of gravity with an inverse law for accelerations $a \ll a_M$ for some constant a_M . A review of MOND is given by Sanders & McGaugh (2002). This is a second order effect, analogous to the gravitational effect of the moon which produces the tides. The second order pioneer effect is a Doppler shift equivalent to an inward acceleration toward the galactic centre and is observed as an apparent modification to orbital velocity. The anomaly is an optical effect arising from the treatment of redshift, not a change to Newtonian dynamics (section 3.3) or evidence of cold dark matter haloes. The accelerations of galaxies in clusters are in the MONDian regime, and after revising the age-redshift relation, offer no immediate evidence that CDM is necessary to explain galaxy evolution.

The MOND test is particularly important for several reasons. Firstly, data fits have been given for over 100 galaxies and thousands of stars, secondly, because cold dark matter does not give any explanation as to why the precisely same acceleration law should be found in galaxies of many sizes and types, thirdly, because halo profiles from evolutionary models and lensing are not consistent with those found from rotation curves, fourthly because there is no satisfactory theory of CDM in

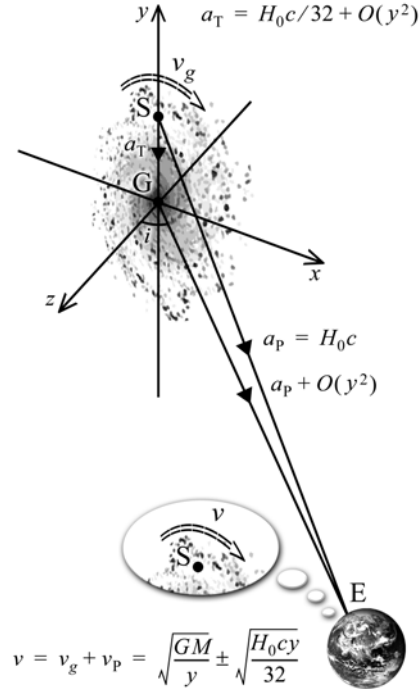


Figure 11: An observer on Earth, E, measures Doppler shift of a star, S, in a galaxy at inclination i° on an axis perpendicular to the Earth. He finds an additional doppler shift equivalent to the rotational velocity associated with inward acceleration $a_T = H_0 c / 32 + O(y^2)$ toward the galactic centre, G.

particle physics, and finally because if galaxies' rotation curves did not obey MOND it would refute this as a 'no CDM' model. In the context of rotation curves the CDM model is further distressed by the dynamical studies of three elliptical galaxies based on the measurement of radial velocities of a large number of planetary nebulae by Romanowsky et al. (2003). They find evidence for "little if any dark matter in these galaxies" and conclude that this does not naturally conform with the CDM paradigm.

A star, S, in a galaxy with centre, G, is subject to an acceleration due to gravity toward G. Doppler shift due to orbital velocity is maximised when S is on a diameter perpendicular to the Earth, E. In addition there is an observed blueshift equivalent to the Pioneer acceleration, $a_P = H_0 c$, toward the Earth. Set up locally Minkowski coordinates with an origin at G with the galaxy in the xy -plane, with the Earth in the xz -plane, and with S at $(0, y, 0)$ (figure 11). The Pioneer blueshift is equivalent to an acceleration which can be resolved into a part $a_P + O(x^2)$ parallel to GE, and a transverse part, a_T , toward G. a_T is independent of galactic mass and would appear in Minkowski coordinates with an origin anywhere in space. For a star on a diameter perpendicular to the Earth, the Doppler shift due to a_T is equivalent to an orbital velocity, v_P , measured relative to quantum coordinates, which are static with respect to the cosmic fluid. v_P is due to expansion and depends on the position of the star, but is independent of its velocity, so that Pioneer shift due to v_P is simply added to Doppler shift due to motion.

Quantum coordinates with metric given by (3.2) are stretched in time by a factor of 2 and in the transverse direction by a factor of 1/2. So the blueshift corresponding to expansion from G is subject to a factor of 1/4. Acceleration is the second time derivative of the transverse distance, and requires a factor of 8 in these coordinates. So we find a net factor of 32, giving a perceived acceleration,

$$a_T = H_0 c / 32 + O(y^2). \quad (7.1)$$

If the corresponding Doppler shift is interpreted as being due to the motion of a body in orbit about G with orbital velocity v_P then, to first order

$$\frac{v_P^2}{y} = \frac{H_0 c}{32} \text{ or } v_P = \pm \sqrt{\frac{H_0 c y}{32}}. \quad (7.2)$$

If the true orbital velocity of S due to gravity is v_g then the observed orbital velocity is

$$v = v_g + v_P = \sqrt{\frac{GM}{y}} \pm \sqrt{\frac{H_0 c y}{32}}. \quad (7.3)$$

(7.3) recognises that, since the alteration to redshift is an optical effect, it is correct to add velocities, not accelerations as would be the case for a dynamical law. Then the apparent acceleration toward G is

$$\frac{v^2}{y} = \frac{GM}{y^2} + \frac{\sqrt{GMH_0 c / 8}}{y} + \frac{H_0 c}{32}. \quad (7.4)$$

The first term on the right hand side of (7.4) is acceleration due to gravity. The last is simply the component of Pioneer acceleration toward G, given by (7.1), and appears also in the absence of a source of gravity. This leaves an apparent acceleration equivalent to a Doppler shift due to velocity,

$$v^2 = \sqrt{GMH_0 c / 8}, \quad (7.5)$$

in agreement with MOND, the phenomenological law proposed by Milgrom (1994) which retains Newton's square law for accelerations $\ddot{y} \gg a_M$ for some constant a_M , but replaces it with

$$\ddot{y} = -(GMa_M)^{1/2} / y \text{ for } \ddot{y} \ll a_M, \quad (7.6)$$

and gives a good match with data. Thus $a_M = H_0 c / 8$. The best fit value of a_M from observations on over a thousand stars is $1 \times 10^{-8} \text{ cm s}^{-2}$, consistent with recent determinations of Hubble's constant and with the value of $H_0 c$ given by Pioneer.

The calculation becomes more subtle in the case of a star in the Milky Way. It is expected that the apparent orbital velocity calculated from Doppler of a star at given radius from the galactic center will vary dependent on the angles subtended from the earth and to the galactic centre. Such a result would be extremely difficult to explain as anything other than an optical distortion. Two new space missions are scheduled for launch, Gaia by the ESA in 2011 and SIM Planetquest by JPL in 2015 (depending on budgetary approval). These will plot the positions and motions of stars in the Milky Way with unprecedented accuracy. It may be hoped that this will provide a rigorous test of the model, since orbital velocities determined from direct measurement of changes in position are predicted to be in agreement with Newtonian dynamics, while Doppler determination should indicate an anomalous acceleration.

8 Big Bang Nucleosynthesis and CBR

The square law applies when all the information about the initial state is contained in the detected light, as in the observation of astronomical bodies. The cosmological microwave background defines a reference frame in which it is continuously observable since decoupling. This scales coordinates as in figure 4b, and the standard linear red shift law applies. The analyses of big bang nucleosynthesis and of decoupling are unaltered, but the density of baryonic matter becomes $0.064 \leq \Omega_B h^2 \leq 0.096$ after normalising Ω_{cr} to 1 according to (5.2). Thus baryonic matter forms 10-20% of critical density, and at an extreme, the ratio of non-baryonic to baryonic matter need only be 4:1 for closure. The prospect remains open that this is within the range of values which might be accounted for by a massive neutrino, particularly after taking into account the change to the age-redshift relation.

The concordance model is supported by the integrated Sachs-Wolfe effect (Afshordi, Loh & Strauss; 2004; Boughn & Crittendon, 2004; Fosalba et al., 2003; Nolte et al., 2004; Scranton et al., 2004) using evidence from the Two-Degree Field Galaxy Redshift Survey (2dFGRS; Peacock et al. 2001; Percival et al., 2001; Efstathiou, 2002), and from the Wilkinson Microwave Anisotropy Probe (WMAP; Spergal, 2003, and references cited therein). In practice these measurements determine cosmological parameters rather than test consistency, and they depend on the distance-redshift relation. Acceleration depends only on distance and time, so that, if the standard model is consistent, a change in the distance-redshift relation can be expected to give a consistent change in the deceleration parameter in different tests in which distance is found from redshift. Thus it is to be expected that $\Omega_s \approx 0.3$ corresponds to $\Omega \approx 1.2$ in the teleconnection model whether it is determined from Supernova or from WMAP and 2dGFS.

The broad properties of the microwave background are unchanged in the teleconnection model, as we expect isotropy and a gaussian random distribution, but it is not possible to interpret the WMAP data as implying that $\Omega_k = 0$, since this may be an artifact of quantum coordinates. McGaugh (2000) has shown that the low amplitude of the second peak in the Boomerang and WMAP data is consistent with a no CDM universe. Spergal comments on discrepancies in the WMAP data on both the largest and smallest scales, and Copi et al (2005) report on unexplained alignments in the data. It is not presently possible to say whether these are caused by higher order corrections in the analysis of data due to the teleconnection; for example it may be necessary to take account of pioneer blueshift when removing foreground contamination.

Acknowledgements

Thanks are due to Bob Day for the supernova fits and for figures 9 and 10, to Erik Anderson for figures 1 to 5 and figure 11, to Oz Hotz de Baar and Philip Helbig for discussions and comments on the manuscript, to Michelle Doherty for advice on the interpretation of extremely red objects and galaxy ageing, and to Peter Francis for his support during the research.

References

- Afshordi N., Loh Y.-S., Strauss M. S., 2004, *Phys. Rev.* **D69**, 083524.
- Anderson J. D., Laing P. A., Lau E. L., Liu A. S., Nieto M. M., Turyshev S. G., 2002, Study of the Anomalous Acceleration of Pioneer 10 and 11, *Phys.Rev.* **D65**, 082004.
- Arcos H. I., Pereira J. G., 2004, *Int.J.Mod.Phys.* D13 2193-2240.
- Astier P. et al., 2005, The Supernova Legacy Survey: Measurement of Ω_M , Ω_Λ and w from the First Year Data Set, accepted in A&A, astro-ph/0510447.
- Benitez N. et al, 2002, *Ap.J.*, **577**, L1-L4
- Boughn S. & Crittendon, 2004, *Nature* **427**, 45.
- Cimatti. et. al., 2004, Old Galaxies in the Young Universe, *Nature*, **430**, 184-188.
- Copi C. J., Huterer D., Schwarz D., Starkman G. D., 2005, *MNRAS*, **000**, 1-27, astro-ph/0508047.
- de Blok, W.J.G., Bosma, A., & McGaugh, S.S. 2003, *MNRAS*, **340**, 657
- Doherty M., Bunker A. J., Ellis R. S., McCarthy P. J., 2005, *MNRAS*, **361** 525-549.
- Efstathiou G., et. al., 2002, *MNRAS*, **330**, L29.
- Einstein A., 1930, Auf die Riemann-metric und den Fern-Parallelismus gegründete einheitliche Field-Theorie, *Math Ann.*, **102**, 658-697.
- Eppeley & Hannah, 1977, *Found. Phys.*, **7**, 51.
- Filippenko A. (2003), Carnegie Observatories Astrophysics Series, Vol. 2: Measuring and Modeling the Universe, ed. W. L. Freedman (CUP)
- Filippenko A. V., 2004, Type Ia Supernova and Cosmology, *White Dwarfs: Probes of Galactic Structure and Cosmology*, ed. E. M. Sion, H. L. Shipman, and S. Vennes (Kluwer: Dordrecht) astro-ph/0410609.
- Fosalba P. et. al., 2003, *ApJ*, **b**, L89.
- Francis C., 2005, Cosmological Redshift in a Relational Quantum Theory, gr-qc/0508077.
- Glazebrook K. et. al., 2004, A high abundance of massive galaxies 3-6 billion years after the Big Bang, *Nature*, **430**, 181-184.
- Knop R. A. et al., 2003, *Astrophys.J.* 598, 102, astro-ph/0309368
- Martel. H. and Shapiro P. R., 2003, Printed 4 March 2006, *Gravitational lensing by CDM halos: singular versus nonsingular profiles*, *MNRAS*, **000**, 1-23, astro-ph/0305174
- McGaugh, S. S., 2000, *Ap.J.*, **541**, L33-L36
- McGaugh, S. S., 2004, *Ap.J.* **611**, 26-39
- Mullis, P. Rosati, G. Lamer, H. Boehringer, A. Schwoppe, P. Schuecker, R. Fassbender, 2005, Discovery of an X-ray-Luminous Galaxy Cluster at $z=1.4$, *ApJ Letters*, **623**, L85-L88, astro-ph/0503004.
- Milgrom M., 1994, *Ann. Phys.*, (NY) **229**, 384 Also see astro-ph/0112069.
- Milgrom M., Sanders R.H., 2005, MOND predictions of "halo" phenomenology in disc galaxies, *MNRAS*, **357**, 45-48
- Misner C. W., Thorpe K. S., Wheeler J. A., 1973, *Gravitation*, Freeman, San Francisco.
- Mörtsell E., Gunnarsson C., Goobar A., 2001, *ApJ*, **561**, 106
- Navarro, J. F., Frenk, C. S., & White, S. D. M. 1997, *ApJ*, **490**, 493
- Nieto M. M., Turyshev S. G., Anderson J. D., 2004, *AIP Conference Proceedings of the 2nd Mexican Meeting on Mathematical and Experimental Physics*, astro-ph/0411077.

- Nolta M. R. et al., 2004, *ApJ*, **608**, 10.
 Park Y., Ferguson H. C., 2003, *ApJ*, **589**, L65-L68, astro-ph/0304317
 Peacock J. A. et al., 2001, *Nature*, **410**, 169.
 Power C., Navarro J. F., Jenkins A., Frenk C. S., White S. D. M., Springel V., Stadel J. and Quinn T., 2003, *The Inner Structure of Λ -CDM Halos I: A Numerical Convergence Study*, *MNRAS* **338**, 14-34, astro-ph/0201544
 Percival W. et al. 2001, *MNRAS*, **327**, 1297.
 Riess A. G. et al, 2004, *Astrophys.J.*, **607**, 665-687.
 Romanowsky, A.J., Douglas, N.G., Arnaboldi, M., Kuijken, K., Merrifield, M.R., Napolitano, N.R., Capaccioli, M., & Freeman, K.C., 2003, *Science*, **301**, 1696
 Sanders R. H. McGaugh S. S., 2002, *Ann. Rev. Astron. Astrophys.*, 40, 263-317.
 Scarpa R., Marconi G. & Gilmozzi R., 2006, *AIP Proceedings*, **822**, *Proceedings of the First Crisis in Cosmology Conference*, astro-ph/0601581.
 Scranton et al, 2004, *Physics Review Letters* astro-ph/0307335.
 Somerville R. S. et. al., 2004, *ApJ*, **600**, L135.
 Steigman G., 2005, Primordial Nucleosynthesis: Successes And Challenges to appear in *Int J. Mod.Phys. E*, astro-ph/0511534.
 Spergal D. L. et. al., 2003, *ApJS*, **148**, 175.
 Swaters, R.A., Madore, B.F., van den Bosch, F.C., & Balcells, M. 2003, *ApJ*, **583**, 732
 Toth V., Turyshev S. G., 2006, gr-qc/0603016
 Turyshev S. G., Viktor T. Toth, Kellogg L. R., Lau, Kyong J. Lee K. J., 2006, *Int.J.Mod.Phys. D15*, 1-56. gr-qc/0512121
 Wayth R. B., Warren S. J., Lewis G. F., Hewett P. C., 2005, The lens and source of the optical Einstein ring gravitational lens ER 0047-2808, *MNRAS*, **360**, 1333-1344, astro-ph/0410253.
 Zhao H, Bacon D. J., Taylor A. N., Horne1 K., 2006, Testing Bekenstein's Relativistic MOND with Lensing, *MNRAS*. **000**, 1–17 Printed 16 December 2005, astro-ph/0509590.

Appendix A Mathematical Description of the Teleconnection

A1 Coordinate Space

Each local region, O , of a continuous manifold, M , can be considered as a subset, $U \subset \mathbb{R}^n$, together with a map, $\psi: U \rightarrow O$. Let U be denoted by axes $\alpha = 0, \dots, n$.

Definition: A coordinate space is any such subset $U \subset \mathbb{R}^n$ together with metric $\eta_{\alpha\beta}$.

Here $\eta_{\alpha\beta}$ is not the physical metric, but is an abstract metric used for mapping. Curvature is naturally conceived in terms of the scaling distortions of a map defined on coordinate space. In general straight lines in coordinate space are not geometrically straight, but for a sufficiently short line segment the deviation from straightness is not detectable, and, to first order, a short rod placed at x will appear as a small displacement vector, A^α , defined, as usual, as the difference in the coordinates of one end of the rod from the other. A coordinate space vector can be defined by inverting the scaling distortions of the map. This is done by choosing primed locally Minkowski coordinates with an origin at x . We define the matrix

$$\kappa^\alpha_{\beta}(x) \equiv x^{\alpha'}_{,\beta}(x). \quad (\text{A1.1})$$

κ is defined using different local Minkowski coordinates for each origin x , so that (A1.1) applies pointwise; it is written as an identity to show that it does not yield a differential equation. It will be assumed that κ is piecewise differentiable.

Definition: For the vector, A^α , at position x , the corresponding coordinate space vector, barred to distinguish it from an ordinary, or physical, vector, is defined by

$$\bar{A}^\alpha(x) \equiv \kappa^\alpha_\beta(x) A^\beta(x). \quad (\text{A1.2})$$

This ensures that the coefficients of a coordinate space vector are equal to the coefficients of the corresponding vector in the primed, Minkowski, coordinates and preserves the inner product:

$$\begin{aligned} \eta_{\mu\nu} \bar{A}^\mu \bar{B}^\nu &= \eta_{\mu\nu} \kappa^\mu_\alpha(x) \kappa^\nu_\beta(x) A^\alpha B^\beta \\ &= \eta_{\mu'\nu'} x^{\mu'}_{,\alpha}(x) x^{\nu'}_{,\beta}(x) A^\alpha B^\beta = g_{\alpha\beta}(x) A^\alpha B^\beta \end{aligned} \quad (\text{A1.3})$$

(A1.3) is true for any vectors A^α , B^α . So

$$g_{\alpha\beta}(x) = \eta_{\mu\nu} \kappa^\mu_\alpha(x) \kappa^\nu_\beta(x). \quad (\text{A1.4})$$

(A1.4) gives the metric in terms of the variable scale coefficients, $\kappa^\mu_\alpha(x)$, of coordinate space vectors compared to physical vectors.

A2 Teleparallel Displacement

A short rod placed at x is described by vector, $A(x)$. An identical short rod is placed at y , so that its coordinate space vector is parallel to $\bar{A}(x)$. It is described by a vector, $A(y)$, whose length is unchanged, $A^2(x) = A^2(y)$. $A(y)$ is teleparallel to $A(x)$ if and only if the coordinate space components are proportional,

$$\kappa^\alpha_\beta(y) A^\beta(y) = \bar{A}^\alpha(y) \propto \bar{A}^\alpha(x) = \kappa^\alpha_\beta(x) A^\beta(x). \quad (\text{A2.1})$$

In general, (A2.1) is not equality because of the different scaling distortions at x and y . (A2.1) generalises Einstein's definition (Einstein, 1930), in which coordinate space is tangent to local Minkowski space at x . In this case axes can be chosen such that $\kappa^\alpha_\beta(x) = \delta^\alpha_\beta$ and (A2.1) reduces to

$$\kappa^\alpha_\beta(y) A^\beta(y) = \bar{A}^\alpha(y) \propto \bar{A}^\alpha(x) = A^\alpha(x) \quad (\text{A2.2})$$

Multiply both sides of (A2.2) by $\eta_{\alpha\gamma} \kappa^\gamma_\mu(y)$ and use (A1.4):

$$A_\mu(y) \propto A^\alpha(x) \eta_{\alpha\gamma} \kappa^\gamma_\mu(y) = A_\gamma(x) \kappa^\gamma_\mu(y). \quad (\text{A2.3})$$

The magnitudes of the left and right hand sides are the same and we have equality,

$$A_\mu(y) = A_\gamma(x) \kappa^\gamma_\mu(y). \quad (\text{A2.4})$$

Parallel transport is a sequence of infinitesimal parallel displacements in the form of (A2.4).

A3 Quantum Coordinates

It is natural to define *quantum coordinates* such that momentum is always teleparallel to momentum observed at the origin.

Definition: In quantum coordinates the plane wave state, $|\bar{p}\rangle$, is defined at any location by replacing 3-vectors with coordinate space 4-vectors, $\bar{p} \equiv (\bar{E}, \bar{p})$ and $\bar{x} \equiv (\bar{t}, \bar{x})$. Then, at time $x^0 = t$,

$$\langle \bar{x} | \bar{p} \rangle = \langle \bar{t}, \bar{x} | \bar{p} \rangle = \left(\frac{1}{2\pi}\right)^{\frac{3}{2}} e^{-i(\bar{E}\bar{t} - \bar{x} \cdot \bar{p})} = \left(\frac{1}{2\pi}\right)^{\frac{3}{2}} e^{-i\bar{x} \cdot \bar{p}}. \quad (\text{A3.1})$$

This definition replaces the affine connection of classical general relativity in the quantum domain. It preserves Newton's first law and the constancy of the speed of light in quantum coordinates. In general teleparallel displacement requires flat coordinate space, but, for light emitted from a distant object at time t and detected at time t_0 , we merely require flatness in the time-radial

plane. If we require spherical symmetry then, for some function, $g: \mathbb{R} \rightarrow \mathbb{R}$, and for some $b \in \mathbb{R}$ the coordinate space metric, η , is

$$ds^2 = b^2(d\tau^2 - d\rho^2) - g^2(\rho)(d\theta^2 + \sin^2\theta d\phi^2). \quad (\text{A3.2})$$

An FRW cosmology can be written in conformally flat coordinates, so that for $a = a(t)$ with $a_0 = a(t_0)$ the metric is

$$ds^2 = \frac{a^2}{a_0^2}(d\tau^2 - d\rho^2 - f^2(\rho)(d\theta^2 + \sin^2\theta d\phi^2)). \quad (\text{A3.3})$$

where the radial coordinate is $r = f(\rho) = \sin \rho, \rho, \sinh \rho$ for a space of positive, zero, or negative curvature respectively, and coordinate time, τ , is related to cosmic time, t , by

$$d\tau = \frac{a_0}{a} dt. \quad (\text{A3.4})$$

Then, for an FRW cosmology in coordinate space given by (A3.2), to first order near the origin, the coordinate space vectors are:

$$\overline{dt} = \frac{1}{b} dt, \overline{dr} = \frac{a}{ba_0} dr, \overline{d\theta} = \frac{f}{g} d\theta, \overline{d\phi} = \frac{f}{g} d\phi. \quad (\text{A3.5})$$

A4 Geodesic Motion

Theorem: In local coordinates with an origin at time $t = t_0$ and with metric

$$ds^2 = dt^2 - dr^2 - r^2(d\theta^2 + \sin^2\theta d\phi^2), \quad (\text{A4.1})$$

for light emitted at time $x^0 = t$ and detected at the origin at time t_0 , momentum is given by

$$\overline{P}_0(x) = -i \frac{a_0^2}{a^2} \overline{\partial}_0, \overline{P}_1(x) = -i \frac{a_0^2}{a^2} \overline{\partial}_1, \overline{P}_2 = \overline{P}_3 = 0. \quad (\text{A4.2})$$

Proof: Light from a distant object is not observable unless $\overline{P}_2 = \overline{P}_3 = 0$. Using (A1.2) and (A3.3), in quantum coordinates, momentum at the time of emission is

$$\overline{P}_0(x) = -i \frac{a_0}{a} \overline{\partial}_0, \overline{P}_1(x) = -i \frac{a_0}{a} \overline{\partial}_1. \quad (\text{A4.3})$$

(A4.2) follows immediately on teleparallel displacement to the origin.

Let k^γ_μ be the scale factors between Minkowski coordinate spaces at x and y , so that

$$k^\gamma_\mu(x) = \frac{a}{a_0} \kappa^\gamma_\mu(y). \quad (\text{A4.4})$$

Then, by (A2.4), parallel displacement from the point x at time $x^0 = t$ to y at time $y^0 = t_0$ yields

$$A_\mu(y) = \frac{a}{a_0} A_\gamma(x) k^\gamma_\mu(y). \quad (\text{A4.5})$$

In the classical correspondence motion may be described as a sequence of states $|f(t_i)\rangle$ at instances $t_i \in T$ with $0 < t_i - t_i < \chi$ in the limit as χ tends to zero. The state at any instant may be regarded as an initial state using coordinates with metric (A3.3). The state at the next instant may be regarded as a final state, which after rescaling, becomes the initial state for the next part of the motion. Momentum is parallel displaced in each coordinate space using (A4.2). Upon rescaling coordinates and renormalisation of energy-momentum, (A4.2) is replaced by

$$P_0(x) = -i \frac{a_0}{a} \partial_0, P_1(x) = -i \frac{a_0}{a} \partial_1, P_2 = P_3 = 0. \quad (\text{A4.6})$$

and (A4.5) gives

$$P_\mu(y) = P_\gamma(x) k^\gamma_\mu(y). \quad (\text{A4.7})$$

When $y = x + dx$ (A4.7) is the standard formula for infinitesimal parallel displacement in a tangent space. The cumulative effect of such infinitesimal parallel displacements is parallel transport. So teleparallelism of momentum between initial and final states in quantum theory, together with renormalisation of momentum, gives rise to parallel transport in the classical domain. Geodesic motion of a classical particle follows as the cumulative effect of displacements in the direction of momentum over small time increments. The same argument holds for a classical beam of light, in which each photon wave function is localised within the beam at any time.